Radiolabeling, Biodistribution, and Dosimetry of ^{123}I-mAb 14C5: A New mAb for Radioimmunodetection of Tumor Growth and Metastasis In Vivo

Christophe M.M. Lahorte, MSc[1]; Klaus Bacher, MSc[2]; Ingrid Burvenich, MSc[1]; Elisabeth D. Coene, PhD[3]; Claude Cuvelier, MD, PhD[3]; Christian De Potter, MD, PhD[3]; Hubert Thierens, PhD[2]; Christophe Van de Wiele, MD, PhD[4]; Rudi A. Dierckx, MD, PhD[4]; and Guido Slegers, PhD[1]

[1]Department of Radiopharmacy, Faculty of Pharmaceutical Sciences, Gent University, Gent, Belgium; [2]Department of Medical Physics and Radiation Protection, Gent University, Gent, Belgium; [3]Department of Pathology, N. Goormaghtigh Institute, Gent University, Gent, Belgium; and [4]Department of Nuclear Medicine, Gent University Hospital, Gent, Belgium.

This study reports on the in vitro evaluation, biodistribution, and dosimetry of ^{123}I-labeled monoclonal antibody (mAb) 14C5, a new antibody-based agent proposed for radioimmunodetection of tumor growth and metastasis in vivo. **Methods:** ^{123}I-mAb 14C5 was prepared by direct iodination and tested for stability in vitro. Binding assays were performed on human SK-BR-3 and HeLa carcinoma cells to investigate the antigen expression, antibody affinity, and kinetics of tracer binding. For the biodistribution and dosimetry study, 3- to 4-wk-old NMRI mice were injected intravenously with ^{123}I-mAb 14C5 (148.0 ± 7.4 kBq per mouse) and killed at preset time intervals. Organs, blood, urine, and feces were counted for radioactivity uptake, and the data were expressed as the percentage injected dose per gram tissue (%ID/g tissue) or %ID. The MIRDOSE3.0 program was applied to extrapolate the estimated absorbed radiation doses for various organs to the human reference adult. **Results:** ^{123}I-mAb 14C5 was obtained in radiochemical yields of 85.0% ± 2.5% and radiochemical purities were >97%. The iodinated antibody demonstrated good in vitro stability with 93.6% ± 0.1% of ^{123}I-mAb 14C5 remaining intact at 24 h after radiolabeling. ^{123}I-mAb 14C5 bound to SK-BR-3 cells (dissociation constant [K_d] ≈ 0.85 ± 0.17 nmol/L) and HeLa cells (K_d ≈ 1.71 ± 0.17 nmol/L) with nanomolar affinity and high specificity, whereas both cell types exhibited a high CA14C5 antigen expression (maximum number of binding sites [B_{max}] = 40.6 ± 5.2 and 57.1 ± 9.6 pmol/L, respectively). In mice, ^{123}I-mAb 14C5 accumulated primarily in lungs (20.4 %ID/g), liver (15.1 %ID/g), and kidneys (11.1 %ID/g) within 5 min after injection. A delayed uptake was observed in stomach (12.8 %ID/g) and urinary bladder (8.7 %ID/g) at 3 and 6 h, respectively, after injection. Radioactivity clearance was predominantly urinary, with 44.9 ± 4.5 %ID excreted during the initial 48 h after administration (cumulative amount). The highest absorbed radiation doses determined for the human reference adult were received by the urinary bladder wall (0.1200–0.1210 mGy/MBq), liver (0.0137–0.0274 mGy/MBq), uterus (0.0196–0.0207 mGy/MBq), and lower large intestine wall (0.0139–0.0258 mGy/MBq). The average effective dose resulting from a single ^{123}I-mAb 14C5 injection was estimated to be 0.017–0.022 mSv/MBq. **Conclusion:** ^{123}I-mAb 14C5 shows good in vitro biologic activity and favorable biodistribution properties for imaging carcinomas of different origin and provides an acceptable radiation dose to the patient.

Key Words: monoclonal antibody 14C5; cell substrate adhesion; metastasis; extracellular matrix; radioimmunodetection

J Nucl Med 2004; 45:1065–1073

The extracellular matrix (ECM) consists of a complex network of macromolecules, such as collagens, glycoproteins, and proteoglycans, which surrounds the connective tissue cells and is mainly being secreted by fibroblasts or other members of the fibroblast family, such as chondroblasts and osteoblasts (*1,2*). Apart from intercellular adhesion (i.e., cell-to-cell adhesion), the organization of cells within connective tissue is based on adhesion of these cells to ECM components (i.e., cell substrate adhesion) (*3*). Subsequently, cell substrate adhesion molecules are considered as essential regulators of cell migration, differentiation, and tissue integrity. They play a role in inflammation, but they also participate in the process of invasion and metastasis of malignant cells in the host tissue (*4–6*). In fact, cell substrate adhesion is a prerequisite for tumor invasion in normal mesenchymal tissue. Invasive tumor cells adhere to the ECM components, such as type IV collagen, laminin, and chondroitin and heparan sulfate proteoglycans, and are guided by them during their permeation through the basal lamina and underlying interstitial stroma of the connective tissue (*7,8*). Several ECM adhesion molecules and their protein receptors have been studied extensively for their

Received Sep. 8, 2003; revision accepted Jan. 15, 2004.

For correspondence contact: Christophe M.M. Lahorte, MSc, Department of Radiopharmacy, Faculty of Pharmaceutical Sciences, Gent University, Harelbekestraat 72, B-9000 Gent, Belgium.

E-mail: christophe.lahorte@ugent.be

involvement in tumor invasion and metastasis, including the integrins, lectins, selectins, and cadherins (*9–12*).

In search of new antibody therapeutics for inhibition of metastatic breast cancer, De Potter et al. (*13,14*) developed several mouse monoclonal antibodies (mAbs) against epitopes on the extracellular membrane of SK-BR-3 human breast cancer cells. One of these mAbs is the IgG1 mAb 14C5, which recognizes an extracellular plasma membrane antigen expressed on SK-BR-3 and MCF-7 human breast cancer cells (*13,14*). The antibody is capable of reversibly inhibiting the adhesion of SK-BR-3 cells on both culture-treated plastic and on pronectin-, fibronectin-, osteopontin-, and vibronectin-precoated culture plates. Furthermore, mAb 14C5 has been shown to prevent invasion and, subsequently, metastasis of SK-BR-3 and MCF-7 cells on host tissue in vitro (*13*). In addition, Giffels et al. (*15*) and Wagner et al. (*16*) demonstrated that mAb 14C5 and its antiidiotypic counterpart (mAb ACA 14C5) significantly inhibit tumor growth in a dose-dependent way in Sprague–Dawley rats bearing HH-16 clone 1/2 adenocarcinomas or fibrosarcomas overexpressing the CA14C5 antigen.

Immunohistochemical evaluation of human benign and malignant neoplastic tissues demonstrated that the 90-kDa CA14C5 antigen is highly expressed in most of the invasive ductal breast carcinomas but also on the cell membrane of several other epithelial malignant tumors, such as spinocellular carcinomas of the head and neck region, lung, skin, and oral mucosa. Adenocarcinomas of the stomach, colon, ovaries, and thyroid gland as well as squamous cell carcinomas also stained strongly positive (*14,17*). An even more pronounced antigen expression was found between and on the cell membrane of fibroblasts surrounding the tumor cells, especially at the invasive front of the tumor even in biopsy specimens in which tumor cells were negative. In general, the antigen was strongly expressed on the cell membrane of both poorly differentiated, highly invasive ductal carcinomas and in situ ductal carcinomas. In contrast, normal multilayered epithelial, muscle, and connective tissues as well as healthy breast tissue stained completely negative (*14*). High antigen expression has also been reported for granulation tissue, suggesting the involvement of CA14C5 in tissue repair and wound healing.

All of these findings suggest that the cancer-associated antigen CA14C5 plays a role in both the construction and the destruction of the connective tissue architecture and ECM and may, in fact, represent a cell substrate adhesion molecule, possibly related to the integrin family (*13*). However, the exact nature of the antigen has not yet been defined. This antigen may serve as a new effective target not only for passive and active cytotoxic immunotherapy but also for radioimmunodetection (RID) and radioimmunotherapy (RIT) of some carcinomas.

This study is focused on the ^{123}I-labeled mAb 14C5 (^{123}I-mAb 14C5) that was recently developed by our group and on the evaluation of its in vitro binding properties to SK-BR-3 and HeLa tumor cells, expressing the CA14C5 antigen (*18*). Since mAb 14C5 is able to prevent cell substrate adhesion and tumor invasion by binding to its antigen, ^{123}I-mAb 14C5 holds promise as a new marker for RID of tumor growth and metastasis by means of SPECT. Because information on the biologic behavior and radiation burden is mandatory for any new radiopharmaceutical before human application, the aim of this feasibility study was to investigate the biodistribution and dosimetry of ^{123}I-mAb 14C5 in mice to establish absorbed radiation dose estimates for the human reference adult by means of the MIRDOSE3.0 program.

MATERIALS AND METHODS

Radiolabeling of ^{123}I-mAb 14C5

The generation and purification of the mouse mAb 14C5 were described previously by De Potter et al. (*13*). Bovine serum albumin (BSA) and other reagents were purchased from Sigma-Aldrich unless stated otherwise. Radiolabeling of the mAb was performed using to the IODO-BEADS method (Pierce Biochemical Co.), as described earlier with minor modifications (*19*). Briefly, before use, IODO-BEADS were washed in 1 mL of 0.01 mol/L potassium phosphate buffer (pH 7.4) and allowed to dry on absorbent paper. Ten micrograms mAb 14C5 in phosphate-buffered saline (PBS) (43.2 mmol/L K_2HPO_4, 9.5 mmol/L $NaH_2PO_4 \cdot H_2O$, and 123.2 mmol/L NaCl, pH 7.4) were added to the reaction vial, buffered with 100 μL 0.1 mol/L potassium phosphate (pH 6.5) and placed in a lead-shielded container. ^{123}I (5.55–222 MBq) in 0.05 mol/L NaOH (Tyco Healthcare) was transferred to the reaction vial and 2 IODO-BEADS were added to the reaction mixture. Radiolabeling was then allowed to proceed for 30 min at room temperature. The iodination of the antibody was terminated by removing the reaction mixture from the vial. IODO-BEADS were washed twice with 500 μL 0.1 mol/L potassium phosphate (pH 6.5) and the wash solutions were added to the reaction mixture. Afterward, ^{123}I-mAb 14C5 was purified by size-exclusion chromatography on a PD10 (G25) Sephadex column (Amersham Pharmacia Biotech) using PBS (pH 7.4), supplemented with 0.25% BSA as eluent. Finally, the chemical and radiochemical purity of the eluted radioligand was determined by high-performance liquid chromatography (HPLC) on a Bio-Silect SEC 250–5 (7.8 × 300 mm) column (Bio-Rad Laboratories) using 0.01 mol/L potassium phosphate (pH 7.4) as the eluent at a flow rate of 0.8 mL/min.

In Vitro Stability of ^{123}I-mAb 14C5

^{123}I-mAb 14C5 was prepared and purified as described, starting with 200 MBq ^{123}I. The radiolabeled antibody was stored at room temperature and aliquots were reinjected on the HPLC column at preset time points (0.5, 1, 3, 6, 21, and 32 h) up to 48 h after radiolabeling. The chemical and radiochemical purity of the injected samples was obtained under HPLC conditions identical to those described for the quality control of the radioligand immediately after purification. All tested time points were investigated in triplicate.

In Vitro Binding of ^{123}I-mAb 14C5 to Carcinoma Cells

Cell Cultures. The following ATCC cell lines were used: SK-BR-3 (breast adenocarcinoma), T47D (breast carcinoma), 791T (skeletal osteosarcoma), HeLa (cervix spinocellular carcinoma), and CoLo-16 (skin spinocellular carcinoma) cells. T47D, 791T, and CoLo-16 cells were cultured in RPMI 1640 medium contain-

ing *N*-(2-hydroxyethyl)piperazine-*N*′-(2-ethanesulfonic acid) (HEPES) and L-glutamine supplemented with 10% fetal calf serum (FCS). SK-BR-3 cells were grown in Eagle's minimal essential medium (EMEM) supplemented with 10% FCS, 60 IU/mL penicillin, 60 IU/mL streptomycin, and 2 mmol/L L-glutamine. Similarly, the culture medium for maintaining HeLa cells consisted of Dulbecco's minimal essential medium (DMEM) supplemented with 10% FCS, 65 IU/mL penicillin, 65 IU/mL streptomycin, and 2 mmol/L L-glutamine. The cell culture media RPMI 1640, EMEM, and DMEM were purchased from Bio-Whittaker, whereas all other cell culture reagents were obtained from Invitrogen.

^{123}I-mAb 14C5 Immunoreactivity to Carcinoma Cells. ^{123}I-mAb 14C5 was initially screened for its binding capacity to SK-BR-3, T47D, 791T, and HeLa carcinoma cells (CA14C5 positive) as well as CoLo-16 cells (CA14C5 negative). Confluent SK-BR-3, T47D, 791T, HeLa, and CoLo-16 cells were washed twice with freshly prepared culture medium and mechanically detached from their culture plates (Nunc). After resuspending and homogenizing in cell culture medium, all cell suspensions were examined microscopically for cell viability, using 20% trypan blue dye (Invitrogen), and for morphology to confirm the absence of multicellular aggregates. Aliquots containing 1.4×10^6 cells in culture medium were then incubated in quadruplicate with 0.45 ± 0.03 nmol/L ^{123}I-mAb 14C5 (150.0 ± 9.0 kBq) for 2 h at 37°C in an atmosphere of 5% CO_2 in air with gentle shaking of the incubation tubes. Afterward, all samples were centrifuged for 8 min at 400*g* at room temperature. The supernatant (SN_1) was withdrawn and the cell pellets washed with PBS (pH 7.4) and centrifuged again at 400*g* for 8 min. The supernatant (SN_2) was again removed and the cell pellet was resuspended with PBS (pH 7.4). Both supernatants and the pellet originating from each sample were counted for radioactivity on a NaI γ-counter (Canberra Packard) to determine the percentage of cell-bound ^{123}I-mAb 14C5. Control samples without carcinoma cells were used to assess nonspecific radioligand binding to the incubation tubes. Specific ^{123}I-mAb 14C5 binding to cells was calculated using Equation 1 to calculate the percentage of specific ^{123}I-mAb 14C5 binding:

$$\%\ \text{specific bound} = \left(\frac{\text{cpm (Pellet)}_{(\text{unknown})}}{\text{cpm (Total)}_{(\text{unknown})}} - \frac{\text{cpm (Pellet)}_{(\text{control})}}{\text{cpm (Total)}_{(\text{control})}}\right) \times 100, \quad \text{Eq. 1}$$

with cpm (Total) = cpm (Pellet + SN_1 + SN_2).

Analysis of Saturation ^{123}I-mAb 14C5 Binding. Immediately after harvesting, aliquots—each containing either 1.4×10^6 SK-BR-3, HeLa, or CoLo-16 cells (as negative control)—were incubated for 1 h with increasing concentrations of ^{123}I-mAb 14C5, ranging from 4.5 ± 0.4 pmol/L to 4.5 ± 0.3 nmol/L final concentration (49.0 ± 4.0 kBq to 49.4 ± 3.9 MBq). Incubation of the samples was performed under conditions identical to those described earlier. Each ^{123}I-mAb 14C5 concentration was investigated in quadruplicate. Analysis of saturation binding was performed according to the method of Bylund and Yamamura et al. (*20*). ^{123}I-mAb 14C5 binding to each cell line was expressed as specific binding versus radioligand concentration. The corresponding values of the dissociation constant (K_d) and the maximum number of binding sites (B_{max}) were generated by curve fitting of the saturation plots applying the GraphPad Prism 3.0 program and were expressed in nmol/L and pmol/L, respectively. The fitted curves, obtained by nonlinear regression analysis, were assumed to follow a 1-site fit unless the statistical analyses within the program indicated that the data gave a significantly better fit using a 2-site model. Additionally, the radioligand binding data (i.e., expressed as bound/free vs. free radioligand concentration) were also expressed as typical Scatchard plots.

Kinetics of ^{123}I-mAb 14C5 In Vitro Binding. To determine the kinetics of radioligand binding to SK-BR-3, HeLa, and CoLo-16 carcinoma cells, binding of ^{123}I-mAb 14C5 over time was studied using a constant radioligand concentration derived from the linear range of the Scatchard plots. SK-BR-3, HeLa, and CoLo-16 cells were harvested from confluent cultures and prepared as described. Samples containing 1.4×10^6 cells in cell culture medium were incubated with 0.45 ± 0.06 nmol/L of ^{123}I-mAb 14C5 (4.8 ± 0.6 MBq) from 5 min to 3 h, at 37°C in an atmosphere of 5% CO_2 in air. Supernatants and cell pellets were processed as described and counted for activity on a NaI γ-counter. Each incubation time interval was investigated in quadruplicate. In addition, the binding experiment was repeated in a similar way for control samples containing no cells to determine nonspecific radioligand binding to the incubation tubes. The results were expressed as the percentage of cell-bound radioligand versus incubation time according to Equation 1.

Biodistribution Studies in Mice

All animal experiments were approved by the local ethics committee of the Gent University, Faculty of Medicine (ethics protocol: Project ECP 00/17) in compliance with the principles of laboratory animal care. For the biodistribution study, 3- to 4-wk-old female NMRI mice ($n = 3$ per time point) (Iffa-Credo) were injected in the lateral tail vein with 148.0 ± 7.4 kBq of research-grade ^{123}I-mAb 14C5 (0.10 ± 0.005 μg mAb 14C5) and killed at preset time points up to 48 h after tracer injection. Selected organs and tissues, blood, as well as urine and feces were collected and tissues were washed with saline. All samples were then counted for radioactivity on a NaI γ-counter (Canberra Packard). The uptake was expressed as the percentage of the injected dose per gram tissue (%ID/g tissue) or as %ID (in particular, for blood and urinary excretion).

Dosimetric Calculations

Mean time–activity curves were generated for the organs of interest. Source organ residence times were determined from integration of the biexponential fit to the experimental biodistribution data. Extrapolation of the animal biodistribution to the human reference adult was performed by assuming that either the %ID/g tissue or the %ID in mice and humans was equal. Absorbed radiation dose estimates were then calculated for the target organs applying the MIRD methodology (*21*) for healthy adults using the MIRDOSE3.0 software package (*22*,*23*).

RESULTS

Radiolabeling and In Vitro Stability of ^{123}I-mAb 14C5

Applying the IODO-BEADS method, ^{123}I-mAb 14C5 could be obtained in radiochemical yields of $85.0\% \pm 2.5\%$ when using starting activities up to 200–222 MBq/10 μg mAb 14C5. Purification of the radioligand on a PD10 (G25) Sephadex column, resulted in a chemical and radiochemical purity of >97% as shown by HPLC analysis. On average, specific activity was in the range of 17.0 ± 1.5 MBq/μg protein. HPLC radiochromatography of the radiolabeled antibody over time demonstrated that $93.6\% \pm 0.1\%$ of

^{123}I-mAb 14C5 was found intact at 24 h after radiolabeling and slowly decreased to 89.7% ± 0.7% at 48 h.

^{123}I-mAb 14C5 Immunoreactivity to Carcinoma Cells

As shown in Table 1, ^{123}I-mAb 14C5 exhibited the highest immunoreactivity toward SK-BR-3 cells and HeLa cells with 3.91% ± 0.08% and 2.26% ± 0.24% of ^{123}I-mAb 14C5 bound to the cells (i.e., total bound minus nonspecifically bound). In contrast, the T47D breast cancer cells (0.100% ± 0.023%) and 791T osteosarcoma cells (0.150% ± 0.009%) showed a significantly lower cell-associated radioactivity. These data were only slightly higher than those observed for the negative control CoLo-16 cells (0.070% ± 0.021%). Nevertheless, cell binding to both T47D and 791T cells was statistically different from that of CoLo-16 cells using a Student *t* test with $P = 0.01$ ($n = 6$). Binding data are presented as a fraction of the specifically bound ^{123}I-mAb 14C5. The CA14C5 expression of all investigated cells and the biologic effect of mAb 14C5 binding on these cells (i.e., cell substrate adhesion inhibition) are given in Table 1.

Analysis of Saturation ^{123}I-mAb 14C5 Binding

Since ^{123}I-mAb 14C5 displayed strongest immunoreactivity to SK-BR-3 and HeLa carcinoma cells, a second set of binding assays was performed, using increasing tracer concentrations, to study the affinity of ^{123}I-mAb 14C5 binding as well as the degree of CA14C5 antigen expression on SK-BR-3 and HeLa cells in detail. CoLo-16 cells were used as negative controls to assess nonspecific cell binding. Analysis of the tracer binding data was based on the method of Bylund and Yamamura et al. (*20*). Saturation of ^{123}I-mAb 14C5 binding to SK-BR-3 and HeLa cells is plotted as specific tracer binding versus tracer concentration in typical saturation plots (Figs. 1A and 1B). Curve fitting of the binding data was performed using nonlinear regression analysis to generate K_d and B_{max} values for each cell type ($r^2 > 0.95$). The corresponding Scatchard plots, shown as insets in Figures 1A and 1B, were derived from the binding data by applying linear regression analysis according to the method of least squares. ^{123}I-mAb 14C5 specifically binds with nanomolar affinity to SK-BR-3 cells ($K_d \approx 0.85 \pm 0.17$ nmol/L) and HeLa cells ($K_d \approx 1.71 \pm 0.17$ nmol/L) and appears to recognize a single binding site. Both carcinoma cell types also exhibited a high CA14C5 antigen expression as reflected by the corresponding B_{max} values derived from the Scatchard plots: $B_{max} = 40.61 \pm 5.19$ pmol/L for SK-BR-3 cells and $B_{max} = 57.08 \pm 9.57$ pmol/L for HeLa cells. Nonspecific binding, as determined by ^{123}I-mAb 14C5 binding to CoLo-16 cells, was low and was comparable to nonpecific radioligand binding to the incubation tubes that did not contain any cells.

Kinetics of ^{123}I-mAb 14C5 In Vitro Binding

The kinetics of ^{123}I-mAb 14C5 binding to SK-BR-3 and HeLa cells was evaluated using a time-dependent binding assay. As shown in the saturation curves (Figs. 2A and 2B), tracer binding to the cells lines proceeds rapidly. The incubation time needed to reach full saturation of the available CA14C5 antigen sites at 37°C was about 2–2.5 h for SK-BR-3 cells and 3 h for HeLa cells, resulting in 3.95% ± 0.23% and 2.36% ± 0.16% specific binding (total bound minus nonspecifically bound), respectively. On the contrary, a very low binding to CA14C5-negative CoLo-16 cells over time was observed.

Biodistribution and Dosimetry in Mice

As shown in Figure 3, ^{123}I-mAb 14C5 was slowly cleared from the blood (9.7 ± 1.4 %ID remaining at 48 h after injection) following a biexponential pharmacokinetic behavior. Fitting of the blood clearance curve was performed with the SPSS 10.0 software package, using the method of least squares, to calculate the biologic half-life ($t_{1/2}$) of the tracer ($r^2 > 0.95$). The biexponential blood clearance of ^{123}I-mAb 14C5 was characterized by a fast phase ($t_{1/2,\alpha} = 1.43 \pm 0.42$ h, 62.8% of total circulating radioactivity in the

TABLE 1
In Vitro Binding of ^{123}I-mAb 14C5 to Carcinoma Cells Compared with CA14C5 Expression and Biologic Activity (Cell Substrate Adhesion Inhibition) of Nonradiolabeled mAb 14C5

Cell line	Origin	CA14C5 expression*	Cell substrate adhesion inhibition†	^{123}I-mAb 14C5 binding‡ (%)	
				Average	SD
SK-BR-3	Breast adenocarcinoma	+++	+++	3.91	0.08
T47D	Breast carcinoma	+	+	0.10	0.02
791T	Skeletal osteosarcoma	+	−	0.15	0.01
HeLa	Cervical spinocellular carcinoma	+++	+	2.26	0.24
CoLo-16	Skin spinocellular carcinoma	−	−	0.07	0.02

*CA14C5 expression based on previously performed immunohistochemical and fluorescent staining experiments (*25,26*).

†Inhibitory effect of nonradiolabeled mAb 14C5 on cell substrate adhesion as demonstrated by earlier reported adhesion inhibition experiments on artificial substrates in vitro (*13,14,25).*

‡Values represent percentage of specific ^{123}I-mAb 14C5 binding to each carcinoma cell type (total bound minus nonspecifically bound) as determined by Equation 1 ($n = 6$).

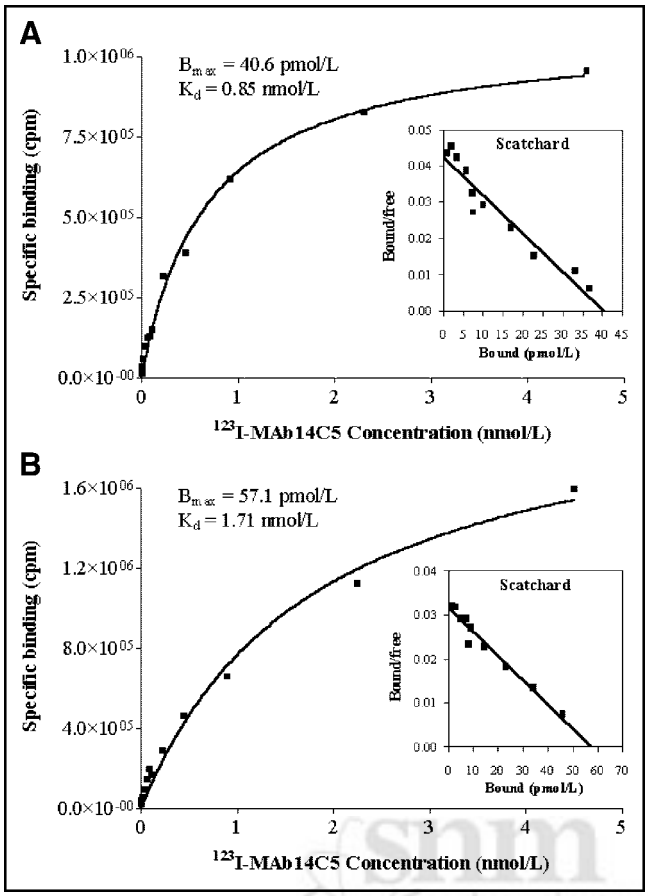

FIGURE 1. Saturation plots for ^{123}I-mAb 14C5 binding to SK-BR-3 cells (A) and HeLa cells (B). Each point represents mean ± SD of 4 measurements. Corresponding curve fittings, as determined by GraphPad Prism 3.0 program, are indicated by solid lines. Insets show respective Scatchard plots derived from linear regression analysis of binding data.

blood) and a slow phase ($t_{1/2,\beta}$ = 130.4 ± 100.0 h, 37.2%). The remaining radioactivity (68 %ID) was rapidly distributed into the extravascular compartments in the initial phase of the tracer biodistribution. Kinetic parameters for blood clearance are presented in Table 2. Blood-pool activity was at any time substantially higher than tracer uptake in any of the other investigated organs. ^{123}I-mAb 14C5 did not cross the blood–brain barrier as indicated by the low brain uptake (<1.0 %ID/g on average). The biodistribution data are presented in Table 3. The highest accumulation of radioactivity occurred in lungs (20.4 ± 3.7 %ID/g), liver (15.1 ± 1.4 %ID/g), and kidneys (11.1 ± 1.1 %ID/g) within 5 min after injection and to a lesser extent in the spleen (9.2 ± 2.4 %ID/g) at 20 min after injection. A delayed uptake was observed in stomach (12.8% ± 2.4 %ID/g) and urinary bladder (8.7 ± 5.2 %ID/g) at 3 and 6 h after injection, respectively (Table 3). ^{123}I-mAb 14C5 was mainly cleared by kidneys, with 40.7 ± 2.9 %ID being excreted in urine at 48 h after injection, representing 90.8% of the total excreted radioactivity. Fecal excretion 48 h after tracer injection (4.1 ± 1.0 %ID) contributed only 9.2% to the total excreted activity as depicted in Figure 3.

Based on the biodistribution data given earlier, time–activity curves were generated for the whole body and several organs of interest, and data were expressed as %ID/g tissue and as %ID. Both types of time–activity curves were fitted using the SPSS 10.0 program to determine mean residence times. The residence times calculated from the biexponential fits for the source organs was highest for the remainder of the body in both dosimetric approaches, followed by the urinary bladder content, liver, and lungs (data not shown).

Mean radiation dose estimates were calculated for the human reference adult using time–activity curves and organ

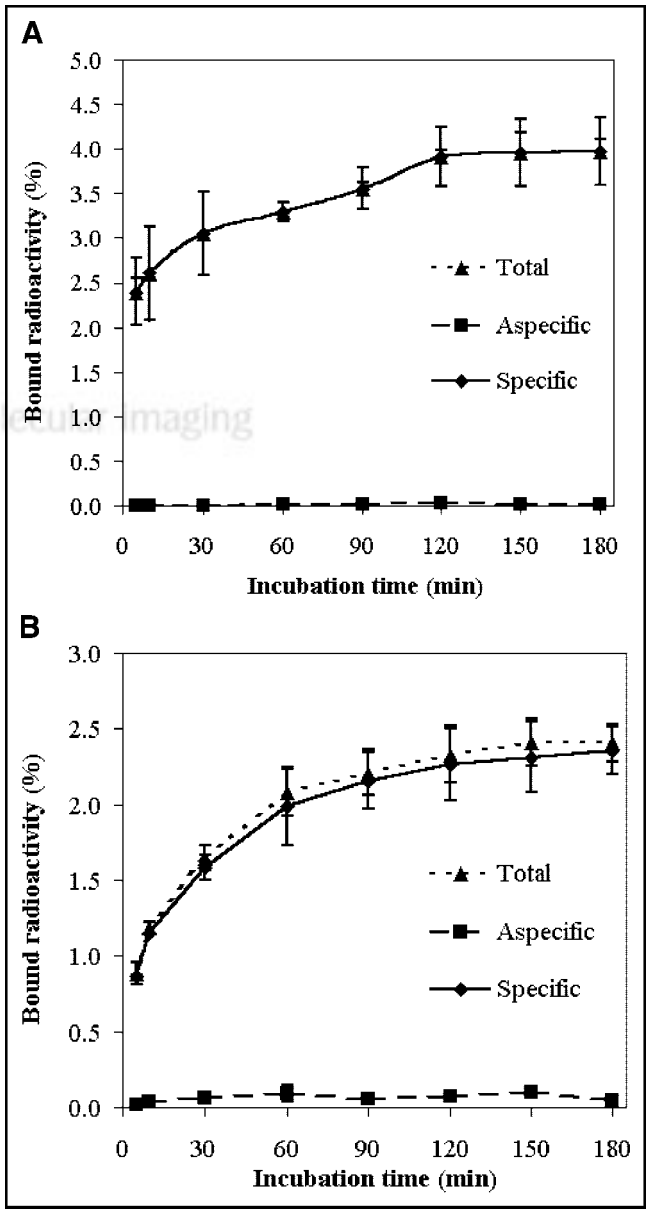

FIGURE 2. In vitro binding of ^{123}I-mAb 14C5 over time to SK-BR-3 cells (A) and HeLa cells (B). Each time point represents mean ± SD of 4 measurements.

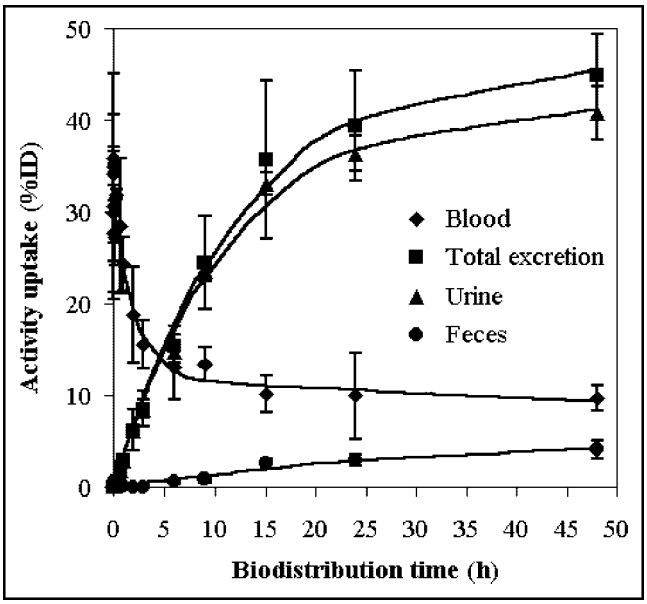

FIGURE 3. Blood clearance (◆) and urinary (▲) and fecal (●) excretion of ^{123}I-mAb 14C5 (%ID) in mice after intravenous injection. Each time point represents mean ± SD of 3 animals. Corresponding curve fittings, as determined by SPSS 10.0 program, are indicated by solid lines.

residence times derived from mice biodistribution data. The MIRDOSE3.0 program was applied assuming that either the %ID/g tissue values or the %ID values for ^{123}I-mAb 14C5 in mice are equal to those in humans. Dosimetry results according to both estimates are given in Table 4. In addition, the absorbed-dose estimate for the urine bladder wall was determined according to the dynamic bladder model as described by Cloutier et al. (*24*). In the applied bladder model, a biologic $t_{1/2}$ of 7.92 h was used with a bladder voiding interval of 4.8 h. The highest absorbed radiation dose was received by the urine bladder wall (0.1200–0.1210 mGy/MBq), liver (0.0137–0.0274 mGy/MBq), and uterus (0.0196–0.0207 mGy/MBq), followed by the lower large intestine wall (0.0139–0.0258 mGy/MBq) and stomach (0.0090–0.0292 mGy/MBq), as determined by the dosimetry estimations used. The predicted radiation dose for the thyroid was in the range of 0.0070–0.0084 mGy/MBq. The effective dose for the human reference adult was estimated to be approximately 0.0172–0.0223 mSv/MBq. When selecting the highest absorbed radiation dose for each organ out of both dosimetry estimations, this worst-case scenario would result in an effective dose of 0.0231 mSv/MBq, which is slightly higher compared with the upper limit value of the estimated effective dose for humans.

DISCUSSION

The immunoreactivity of ^{123}I-mAb 14C5 correlates well with the CA14C5 expression status of the investigated cells. This is in agreement with the previously reported immunohistochemistry data (Table 1) (*25*,*26*). SK-BR-3 and HeLa cells, strongly positive for the CA14C5 antigen, exhibited the highest tracer binding. T47D and 791T cells, characterized by a moderate-to-weak CA14C5 staining, showed low ^{123}I-mAb 14C5 binding, almost at the same level of tracer binding to CA14C5-negative CoLo-16 cells. Visual assessment of the antigen expression by means of immunohistochemical staining is difficult to correlate accurately with quantitative methods, such as tracer binding assays. No true correlation was found between ^{123}I-mAb 14C5 binding to T47D, 791T, and HeLa cells and the known biologic effect (cell substrate adhesion inhibition) that nonradiolabeled mAb 14C5 exerts on these cell lines (Table 1). Only for SK-BR-3 cells was a positive correlation found between both parameters.

The in vitro affinities of ^{123}I-mAb 14C5 are in the range of affinities observed for radiolabeled antibodies or somewhat better by a factor of 2.9–5.9 than the nanomolar affinity, K_d = 5 nmol/L, of trastuzumab (Herceptin; Genentech, Inc.) for breast cancer cells expressing the HER-2/neu receptor as reported by Coussens et al. (*27*) and Press et al. (*28*). Since binding affinities of better than 10^{-8} mol/L and receptor densities of 50,000–100,000 binding sites per tumor cell are considered as one of the requirements for efficient in vivo detection of solid tumors, RID of CA14C5-positive human carcinomas with ^{123}I-mAb 14C5 seems achievable (*29*). However, it should be noted that the stroma surrounding the tumor cells often expresses higher levels of the CA14C5 antigen than that of the tumor cells. Previous immunohistochemical evaluation of tumor biopsy specimens clearly demonstrated that the strong signal of the connective tissue can be attributed to pronounced antigen expression in extracellular spaces and on the cell membrane of fibroblasts surrounding tumor cells, especially at the invasive front of the tumor (*13*,*14*). In some biopsy specimens, strong positive staining of the stroma was not accompanied by any staining of the tumor cells. In general, poorly differentiated, highly invasive ductal carcinomas showed the strongest staining (the stroma and both the tumor cell membranes and their cytoplasmic membrane extensions)

TABLE 2
Kinetic Parameters for Blood Clearance of ^{123}I-mAb 14C5 in Mice

Parameter	Average	SD
A_α	20.29	2.45
$t_{1/2,\alpha}$ (h)	1.43	0.42
A_β	12.03	2.41
$t_{1/2,\beta}$ (h)	130.42	100.00
r^2	0.95	

A_α and A_β represent activity fractions (%ID) in blood at any time (T) after tracer injection, corresponding to biologic half-lives $t_{1/2,\alpha}$ and $t_{1/2,\beta}$, respectively.

Clearance data were fit to the following equation using method of least squares: Activity = $A_\alpha \cdot e^{-(0.693T/t_{1/2,\alpha})} + A_\beta \cdot e^{-(0.693T/t_{1/2,\beta})}$.

compared with in situ ductal carcinomas, in which the antigen was only expressed on the cell membrane of the tumor cells (*13,14*). These histologic findings imply that the ^{123}I-mAb 14C5 uptake in tumors could be considerably higher than that predicted from the B_{max} values. Furthermore, it can expected that the extent of tracer uptake by tumors in vivo might correlate with the degree of differentiation and the invasive character of the investigated tumor.

Immunohistochemical evaluation of human benign and malignant neoplastic tissues has previously shown that the CA14C5 antigen is highly expressed in most of the invasive ductal breast carcinomas but also on the cell membrane of several other epithelial malignant tumors, such as spinocellular carcinomas of the head and neck region, lung, skin, and oral mucosa. Adenocarcinomas of the stomach, colon, ovaries, and thyroid gland as well as squamous cell carcinomas also stained strongly positive (*14,17*). Therefore, mAb 14C5 and radioimmunoconjugates thereof could offer much broader perspectives in (radio)immunotherapy and in vivo detection of cancer in addition to metastatic breast cancer therapy. CA14C5-negative tumors also might benefit from the treatment with unlabeled or radiolabeled mAb 14C5, since the connective tissue surrounding the tumor cells has also been shown to express the CA14C5 antigen.

When compared with ^{18}F-FDG PET, in vivo imaging of CA14C5 tumor antigen expression could provide in vivo histopathologic information for diagnostic purposes, for targeted radionuclide therapy, and for therapy follow-up. With regard to therapy follow-up, in vivo imaging of changes over time in CA14C5 tumor expression, after instigation of specific "cytostatic" treatments targeting the underlying molecular abnormalities responsible for invasion and metastasis of human malignancies, might prove a more appropriate endpoint for treatment monitoring compared with volumetric changes as visualized by CT and MRI.

The biodistribution study in NMRI mice demonstrates that ^{123}I-mAb 14C5 is cleared from the blood compartment in $t_{1/2,\beta} = 130.42 \pm 100.00$ h). This slow blood clearance can be attributed to the fairly high molecular weight of the protein (150 kDa) and is comparable with existing radiolabeled antibodies that are generally known to exhibit a slow clearance from the blood compartment. As a result, blood-pool activity was at any time higher than tracer uptake in any of the other investigated organs (Table 3). In fact, an overall low tracer uptake was observed in most organs that, combined with a sufficient tumor uptake, should provide good imaging conditions for in vivo detection of CA14C5-expressing tumors and their subsequent metastases, not only in the thoracic or abdominal region but also in other regions, such as the head and neck region, skin, and oral mucosa. From the dosimetric point of view, the fairly high retention of activity in the blood compartment can also be considered as a benefit since the tracer distribution in the whole body—and, subsequently, the radiation burden to various organs—is thereby being decreased substantially.

TABLE 3
Biodistribution Results (%ID/g tissue) for ^{123}I-mAb 14C5 in NMRI Mice ($n = 3$)

Tissue	Biodistribution time (h)								
	0.083	0.33	1	3	6	9	15	24	48
Blood	51.13 ± 2.38	48.19 ± 4.38	38.62 ± 1.02	31.28 ± 2.06	27.02 ± 2.09	21.51 ± 2.54	16.01 ± 3.91	14.33 ± 3.06	13.31 ± 1.39
Brain	1.26 ± 0.26	0.93 ± 0.02	0.90 ± 0.25	0.71 ± 0.08	0.66 ± 0.17	0.46 ± 0.18	0.32 ± 0.15	0.28 ± 0.05	0.27 ± 0.08
Heart	8.08 ± 1.94	8.74 ± 2.13	7.96 ± 0.74	4.24 ± 3.56	6.81 ± 1.78	5.23 ± 1.82	3.57 ± 1.21	2.98 ± 0.59	2.42 ± 0.05
Lungs	20.39 ± 3.74	20.29 ± 11.55	16.69 ± 3.58	10.96 ± 3.58	7.83 ± 1.01	6.24 ± 1.50	4.91 ± 1.41	4.00 ± 1.09	3.46 ± 1.06
Stomach	5.72 ± 3.37	6.88 ± 2.12	7.35 ± 2.98	12.78 ± 2.44	11.51 ± 7.49	5.99 ± 2.93	0.87 ± 0.06	1.10 ± 0.25	1.02 ± 0.68
Spleen	8.45 ± 0.41	9.21 ± 2.36	6.69 ± 0.50	5.79 ± 0.84	4.78 ± 0.79	3.73 ± 0.38	3.01 ± 1.14	2.27 ± 0.39	2.13 ± 0.80
Liver	15.12 ± 1.40	14.24 ± 0.65	10.58 ± 1.35	9.17 ± 0.96	7.95 ± 1.57	5.91 ± 0.59	3.68 ± 1.46	3.15 ± 0.31	2.69 ± 0.55
Kidneys	11.13 ± 1.07	9.57 ± 0.81	9.16 ± 0.93	7.88 ± 0.67	6.21 ± 0.63	4.66 ± 1.18	3.32 ± 1.21	2.99 ± 0.66	2.62 ± 0.17
Small intestines	2.01 ± 0.48	2.17 ± 0.39	3.11 ± 0.20	3.67 ± 0.06	3.30 ± 0.89	2.27 ± 0.24	1.23 ± 0.37	1.12 ± 0.25	0.92 ± 0.23
Large intestines	1.12 ± 0.32	1.04 ± 0.21	1.32 ± 0.16	2.17 ± 0.22	2.39 ± 0.53	1.96 ± 0.37	0.93 ± 0.25	0.84 ± 0.06	0.80 ± 0.19
Bladder	2.29 ± 0.82	2.67 ± 0.72	3.48 ± 2.50	5.76 ± 3.52	8.68 ± 5.16	7.68 ± 2.68	4.26 ± 1.14	3.74 ± 0.72	3.43 ± 2.61
Body remainder	3.44 ± 0.48	3.28 ± 0.57	3.66 ± 0.48	4.10 ± 0.40	4.11 ± 0.23	3.46 ± 0.25	2.79 ± 0.45	2.90 ± 0.21	2.81 ± 0.29
Excretion*	0.15 ± 0.24	0.24 ± 0.62	3.38 ± 1.75	7.22 ± 0.81	13.76 ± 3.00	28.03 ± 3.41	45.98 ± 9.64	43.55 ± 6.75	48.05 ± 5.24

*Excretion values (urine + feces) are expressed as %ID.

TABLE 4
Radiation Absorbed-Dose Estimates (mGy/MBq) for ^{123}I-mAb 14C5 for Target Organs

Target organ	$\%ID/g_{mice} = \%ID/g_{humans}$ Average	SD	$\%ID_{mice} = \%ID_{humans}$ Average	SD
Adrenals	0.01020	0.00152	0.01140	0.00305
Brain	0.00299	0.00032	0.00275	0.00033
Breasts	0.00641	0.00058	0.00570	0.00071
Gallbladder wall	0.01120	0.00226	0.01510	0.00565
LLI wall	0.01390	0.00079	0.02580	0.00364
Small intestine	0.01150	0.00208	0.02490	0.01270
Stomach	0.00899	0.00164	0.02920	0.01380
ULI wall	0.01050	0.00130	0.02440	0.00625
Heart wall	0.00903	0.00211	0.01340	0.00437
Kidneys	0.01210	0.00370	0.02400	0.00958
Liver	0.01370	0.00774	0.02740	0.01820
Lungs	0.01320	0.00489	0.01020	0.00379
Muscle	0.00878	0.00061	0.00846	0.00107
Ovaries	0.01370	0.00079	0.01630	0.00288
Pancreas	0.01060	0.00142	0.01360	0.00394
Red marrow	0.00816	0.00063	0.00804	0.00118
Bone surfaces	0.01480	0.00102	0.01370	0.00155
Skin	0.00583	0.00035	0.00525	0.00049
Spleen	0.01000	0.00124	0.01730	0.00317
Testes	0.01000	0.00034	0.00897	0.00036
Thymus	0.00851	0.00071	0.00751	0.00082
Thyroid	0.00839	0.00045	0.00704	0.00039
Urine bladder wall	0.12100	0.00084	0.12000	0.00147
Uterus	0.01960	0.00075	0.02070	0.00241
Total body dose	0.00926	0.00090	0.00955	0.00177
Effective dose (mSv/MBq)	0.01720	0.00178	0.02230	0.00483

LLI = lower large intestine; ULI = upper large intestine.

All of these findings seem to reflect the generally observed hepatic uptake and urinary excretion of radiolabeled proteins, their related metabolites, and trapping of some free iodine by the stomach. In spite of the predominant urinary excreted radioactivity, the cumulative excreted activity over time remains relatively low and can be attributed to the high molecular weight of the radioligand. Subsequently, the rather slow urinary excretion results in a radiation dose estimate for kidneys and urine bladder wall in humans of 0.0121–0.0240 and 0.1200–0.1210 mGy/MBq administered, respectively. In contrast, low-molecular-weight antibody fragments or peptides are generally being excreted through kidneys and urine much faster and to a substantially higher extent.

Initially, the predominant lung uptake very early after ^{123}I-mAb 14C5 administration might seem to limit the usefulness of the molecule for imaging tumor invasion in the thoracic region—for example, invasive ductal breast carcinomas, lung spinocellular carcinomas, or adenocarcinomas of the thyroid gland. However, the favorable kinetics of tracer clearance from the lungs should result in good imaging conditions for this region at later time points (>2 h) after injection. If the fairly high retention of activity in the blood is taken into account, delayed imaging of tumor uptake in this region may be required anyway, to increase target-to-background ratios. On the other hand, imaging of tumors in the abdominal region—for example, adenocarcinomas of the colon, stomach, and ovaries—around 3–6 h after injection might be impeded somehow due to interfering bowel activity originating in the stomach and liver. In this regard, the presence of a strong tracer uptake in abdominal tumors might be a prerequisite for in vivo imaging of tumor invasion and metastasis during that time frame in this particular region. Alternatively, tumor uptake of the radioligand in the abdomen could easily be assessed at earlier or later time points considering the physical $t_{1/2}$ of ^{123}I (13.2 h). The moderate accumulation of radioactivity in the abdominal region might be explained by the occurrence of some enterohepatic clearance. Alternatively, this activity uptake could indicate slowly ongoing deiodination of ^{123}I-mAb 14C5 in vivo, with the production of some free iodine and its subsequent trapping in the stomach. However, the low absorbed radiation dose estimate for the thyroid, as determined by the dosimetry study, does not seem to reflect any significant formation of free iodine due to deiodination of the ^{123}I-mAb 14C5 so far. In any case, these assumptions remain to be verified by human biodistribution studies with the tracer since species differences in the metabolism of radiolabeled proteins between laboratory animals and humans have been reported previously.

The MIRDOSE software provides a calculation of the effective dose for human adults as defined in the ICRP Publication 60 (*30*). Based on the estimated effective dose of 0.017–0.022 mSv/MBq obtained in our dosimetry study, both patients and volunteers could easily be investigated with 222 MBq ^{123}I-mAb 14C5, allowing planar and SPECT imaging. Subsequently, the corresponding effective dose of 3.8–4.9 mSv is still 12%–32% lower compared with the reported average effective dose per patient from nuclear medicine procedures in Europe (*31*). As a result of the moderately low effective dose, ^{123}I-mAb 14C5 could be administered in doses up to 230–295 MBq before reaching the 5-mSv upper-limit average effective dose of Category IIb of ICRP Publication 62 (*32*). To our knowledge, these dosimetry data provide the first evidence that ^{123}I-mAb 14C5 could be applied safely in humans near the 300-MBq level and, therefore, should allow further evaluation of the radiolabeled antibody in future clinical trials without causing substantial radiotoxicity to the vital organs.

CONCLUSION

In summary, ^{123}I-mAb 14C5 can be produced in high radiochemical yields and purities while maintaining good in vitro stability over time. The tracer was shown to bind with high specificity and nanomolar affinity to SK-BR-3 and HeLa carcinoma cells, which were both characterized by a high CA14C5 receptor density. Therefore, efficient RID of

such tumor types in vivo by means of ^{123}I-mAb 14C5 seems feasible. The favorable biodistribution characteristics of the tracer, in combination with a sufficient tumor uptake, should provide good imaging conditions in the thoracic or abdominal region when studying carcinomas of different origin. Furthermore, the estimated effective dose for human adults should easily allow safe administration of megabecquerel (millicurie) amounts of ^{123}I-mAb 14C5 for the performance of human clinical trials. ^{123}I-mAb 14C5 could offer new perspectives for RID of primary and metastatic breast cancer, but also spinocellular carcinomas of the head and neck region, of the lungs, skin, and stomach, and colon and ovarian carcinomas. Additionally, radioimmunoconjugates of mAb 14C5 or smaller fragments thereof with β-emitting radionuclides, such as ^{131}I, ^{90}Y, or ^{188}Re, could provide new approaches in RIT of breast cancer metastasis and other types of carcinomas by specific targeting of cell substrate adhesion molecules involved in tumor growth and invasion.

REFERENCES

1. Kreis T, Vale R. *Guidebook to the Extracellular Matrix, Anchor, and Adhesion Proteins.* Oxford, UK: Oxford University Press; 1999.
2. Alberts B, Bray D, Lewis J, Raff M, Roberts K, Watson JD. Cell junctions, cell adhesion, and the extracellular matrix. In: Alberts B, Bray D, Lewis J, Raff M, Roberts K, Watson JD, eds. *Molecular Biology of the Cell.* 3rd ed. New York, NY: Garland Publishing; 1994:chapter 19, part IV.
3. Jockusch BM, Bubeck P, Giehl K, et al. The molecular architecture of focal adhesions. *Annu Rev Cell Dev Biol.* 1995;11:379–416.
4. Jiang WG, Puntis MC, Hallett MB. Molecular and cellular basis of cancer invasion and metastasis: implications for treatment. *Br J Surg.* 1994;81:1576–1590.
5. Albelda SM. Role of integrins and other cell adhesion molecules in tumor progression and metastasis. *Lab Invest.* 1993;68:4–17.
6. Cavallaro U, Christofori G. Cell adhesion in tumor invasion and metastasis: loss of the glue is not enough. *Biochim Biophys Acta.* 2001;1552:39–45.
7. Yurchenco PD. Assembly of laminin and type IV collagen into basement membrane networks. In: Yurchenco PD, Birk DE, Mecham RP, eds. *Extracellular Matrix Assembly and Structure.* San Diego, CA: Academic Press; 1994.
8. Anderson JC. Biochemical basis of connective tissue disease. In: Gardner DL, ed. *Pathological Basis of the Connective Tissue Diseases.* London, UK: Arnold; 1992:173–226.
9. Behrens J. The role of cell adhesion molecules in cancer invasion and metastasis. *Breast Cancer Res Treat.* 1993;24:175–184.
10. Dedhar S, Saulnier R. Alterations in integrin receptor expression on chemically transformed human cells: specific enhancement of laminin and collagen receptor complexes. *J Cell Biol.* 1990;110:481–489.
11. Pignatelli M, Cardillo MR, Hanby A, Stamp GW. Integrins and their accessory adhesion molecules in mammary carcinomas: loss of polarization in poorly differentiated tumors. *Hum Pathol.* 1992;23:1159–1166.
12. Takeichi M. Cadherin cell adhesion receptors as a morphogenetic regulator. *Science.* 1990;251:1451–1455.
13. De Potter C, Schelfhout AM, De Smet FH, et al. A monoclonal antibody directed against a human cell membrane antigen prevents cell substrate adhesion and tumor invasion. *Am J Pathol.* 1994;144:95–103.
14. Coene E, Schelfhout AM, De Ridder L, De Potter C. Generation of a monoclonal antibody directed against a human cell substrate adhesion molecule and the expression of the antigen in human tissues. *Hybridoma.* 1997;16:77–83.
15. Giffels P, Köhler S, De Potter C, et al. MAb 14C5 against a human cell substrate adhesion molecule for inhibition of tumor growth in-vivo [abstract]. *Eur J Cancer.* 1997;33(suppl 5):96.
16. Wagner U, Köhler S, Prietl G, et al. Monoclonal anti-idiotype antibodies in immunotherapy of ovarian carcinoma (MAb ACA125) and breast carcinoma (MAb ACA14C5) [in German]. *Zentralbl Gynakol.* 1999;121:190–195.
17. Coene E, Willems K, Verbiest L, Wagner U, Schlebusch H, De Potter C. Expression patterns and functional activity of the human 14C5 cell substrate adhesion molecule [abstract]. *Eur J Cancer.* 1997;33(suppl 5):96.
18. Lahorte C, Burvenich I, Bacher K, et al. Synthesis, biodistribution and dosimetry of the ^{123}I-14C5 MoAb in mice: a potential SPECT-ligand for radio-immunodetection of tumour growth and metastasis in vivo [abstract]. *Eur J Nucl Med.* 2002;29(suppl 1):S77.
19. Lahorte C, Dumont F, Slegers G, Van De Wiele C, Dierckx RA, Philippé J. Synthesis and in vitro stability of ^{123}I-labelled annexin V: a potential agent for SPECT imaging of apoptotic cells. *J Labelled Compds Radiopharm.* 2000;43:739–751.
20. Bylund DB, Yamamura HI. Methods for receptor binding. In: Yamamura HI, ed. *Methods in Neurotransmitter Receptor Analysis.* New York, NY: Raven Press; 1990:1–35.
21. Loevinger R, Budinger T, Watson E. *MIRD Primer for Absorbed Dose Calculations.* New York, NY: The Society of Nuclear Medicine; 1991:1–17.
22. Cristy M, Eckerman K. *Specific Absorbed Fractions of Energy at Various Ages From Internal Photon Sources.* ORNL/TM-8381/VII. Oak Ridge, TN: Oak Ridge National Laboratory; 1987:7–29.
23. Stabin MG. MIRDOSE: personal computer software for internal dose assessment in nuclear medicine. *J Nucl Med.* 1996;37:538–546.
24. Cloutier RJ, Smith SA, Watson EE, Snyder WS, Warner GG. Dose to the fetus from radionuclides in the bladder. *Health Phys.* 1973;25:147–161.
25. Vanholme B. Detection and purification of a cell substrate antigen involved in the invasion and metastasis of breast cancer [dissertation]. Gent, Belgium: Gent University; 1999.
26. Burvenich I. Characterization of the 14C5 antigen involved in cell substrate adhesion, invasion and metastasis of breast carcinoma cells [dissertation]. Gent, Belgium: Gent University; 2001.
27. Coussens L, Yang-Feng TL, Liao YC, et al. Tyrosine kinase receptor with extensive homology to EGF receptor shares chromosomal location with neu oncogene. *Science.* 1985;230:1132–1139.
28. Press MF, Pike MC, Chazin VR, et al. Her-2/neu expression in node-negative breast cancer: direct tissue quantification by computarized image analysis and association of overexpression with increased risk of recurrent disease. *Cancer Res.* 1993;53:4960–4970.
29. Fischman AJ, Khaw BA, Strauss HW. Quo vadis radioimmune imaging. *J Nucl Med.* 1989;30:1911–1915.
30. International Commission on Radiological Protection. *1990 Recommendations of the International Commission on Radiological Protection.* ICRP Publication 60. *Ann ICRP.* Oxford, UK: Pergamon Press; 1991;21:6–10.
31. Beekhuis H. Population radiation absorbed dose from nuclear medicine procedures in the Netherlands. *Health Phys.* 1988;54:287–291.
32. International Commission on Radiological Protection. *Radiological Protection in Biomedical Research.* ICRP Publication 62. *Ann ICRP.* Oxford, UK: Pergamon Press; 1991;22:12–13.